J MATER SCI **41** (2006) 2647–2657

Comparison of glide mechanisms in hcp Ti and Ti_3Al

MARC LEGROS, ALAIN COURET, DANIEL CAILLARD
CEMES-CNRS, 29 Rue J. Marvig, BP 4347, 31 055, Toulouse, Cedex 4, France

Published online: 17 April 2006

Several dislocation glide mechanisms are studied in Ti and Ti_3Al by means of *in situ* straining experiments in a transmission electron microscope at various temperatures. The prismatic glide of α titanium occurs by the jerky motion of straight screw **a**-dislocations subjected to a frictional force. An explanation for the discontinuity in the temperature dependence of the corresponding activation area is proposed, on the basis of the experimentally measured variation of the corresponding dislocation jump length. In Ti_3Al, superlattice 2**a**-dislocations exhibit two different dissociation modes in prismatic planes corresponding to highly different antiphase boundary energies. The properties of these two types of dislocation are compared and discussed. It is shown that the motion of $2\mathbf{c}+\mathbf{a}$ superlattice dislocations in pyramidal planes is controlled by a new mechanism: the self-nucleation of small-size obstacles as the result of irreversible atomic displacements. The tension/compression asymmetry observed between type 1 and type 2 pyramidal planes is finally discussed.

1. Introduction

Titanium, zirconium and magnesium alloys as well as Ti-based intermetallic alloys are still attracting a great deal of interest in materials science. The understanding of their mechanical properties requires a deep knowledge of the corresponding elementary deformation mechanisms. In a previous contribution, the glide mechanisms in the prismatic planes of magnesium and beryllium were studied by *in situ* straining experiments in the transmission electron microscope [1]. The aim of the present work is to make a review of the same analyses in the prism, basal and pyramidal planes of α Ti and Ti_3Al. The structure and the properties of dislocations in hcp metals and alloys have been recently reviewed by Numakura and Koiwa [2] and will not be described again in the present paper.

2. Experimental

To study these deformation mechanisms, *in situ* straining experiments have been performed at various temperatures in JEOL 200CX and JEOL 2010HC electron microscopes. Several straining holders have been designed for low-temperature and high-temperature deformation [3, 4]. Microsamples are 3 mm $\times$ 1 mm rectangles with a thickness of 0.1 mm, mechanically polished, and perforated by a thin edged hole. They are glued on a copper grid or on anchoring rings that are subsequently fixed onto the jaws of the holder. We know from experience and from finite element calculations [3] that (i) deformation starts where the macroscopic straining axis is tangent to the thin-edged hole and (ii) the corresponding local straining axis is parallel to the macroscopic one within $\pm 10^\circ$, so that the Schmid law should apply, when the thin areas do not contain cracks.

In practice, thin-foil effects can be avoided provided several of the following conditions are fulfilled: (i) the foil thickness is larger than the radius of curvature of the dislocations under stress, (ii) important mechanisms are initiated far enough from the surfaces (namely at a distance equal to or larger than the radius of curvature), (iii) the observed mechanisms are identical for several foil planes containing the same straining axis, (iv) the local stress (deduced from dislocation radii of curvature) is similar to that measured in macroscopic mechanical tests at various temperatures, and/or (v) observations are consistent with results obtained by other methods. Most of these conditions were satisfied in the experiments described in this article.

3. Prismatic glide in α titanium

Glide of dislocations with Burgers vector $\mathbf{a} = 1/3\langle 11\bar{2}0\rangle$ (and hereafter called **a**-dislocations) has been observed between 100 K and 473 K in α titanium containing two different impurity levels: high-purity titanium provided

0022-2461
DOI: 10.1007/s10853-006-7828-5

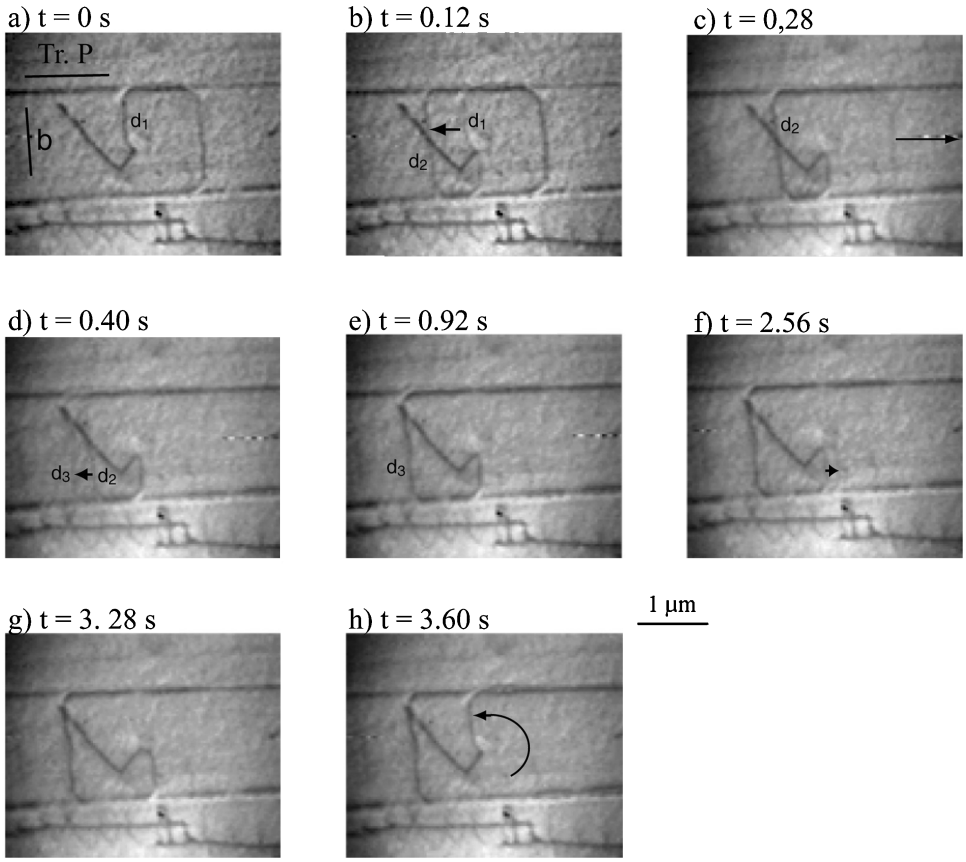

Figure 1 Polar source emitting dislocations with an **a**-type Burgers vector in a prismatic plane of a medium purity titanium. *In situ* straining experiment at room temperature. "Tr P" is the trace of the prismatic plane, *b* is the direction of the Burgers vector (in projection). Jumps between locking positions are arrowed.

by Biget and Saada [5], containing 50 ppm of oxygen and 70 ppm of iron, and moderate-purity titanium provided by Naka *et al*. [6], containing 3270 ppm of equivalent oxygen atoms ($O^* = C + 2N + O$). Depending on the sample orientation, dislocations either glide in a single prismatic plane, or cross slip between various planes (prismatic, basal, pyramidal) [7, 8].

3.1. Prismatic glide

Fig. 1 shows a polar source emitting **a**-dislocations in a prismatic plane of the medium-purity titanium strained at room temperature. From the rectilinear shape of the slip traces, it can be deduced that these dislocations glide strictly in the prismatic plane. They exhibit very straight screw portions indicating the presence of a strong frictional force. Numbers 1 to 4 refer to the segments emitted by the source, and the subscript letters refer to the successive positions of each dislocation. Let's follow the movement of segment *d* emitted to the left. It glides by a series of jumps between locking positions (d_1, d_2 and d_3). In each case, the initial and final positions of the jump can be seen on the corresponding video frame, namely picture *b* for the jump between d_1 and d_2, and picture *d* for that between d_2 and d_3. The jump time is thus always much smaller than one fiftieth of a second. The waiting time is variable. For instance, in the medium-purity titanium strained at 230 K, it varies between one tenth of a second and several tens of seconds [7].

Jerky motion of **a**-dislocations in prismatic planes has been observed in the entire range of temperature investigated, in Ti of both purities. The average jump length decreases with increasing temperature and reaches its lowest value (the interatomic distance) at approximately 350 K in low-purity Ti (Fig. 2). A similar behaviour has been observed in high-purity Ti.

3.2. Cross-slip between prism, pyramidal and basal planes

For specific orientations of the local stress, cross-slip has been observed between prism planes, pyramidal planes of the first type, and more scarcely the basal plane. This behaviour is observed in Fig. 3 where a polar source emits two loops in high purity titanium strained at room temperature. Here again, mobile screw dislocations are very rectilinear and move jerkily. Fig. 3g shows slip traces left by dislocations, the average directions of which are neither

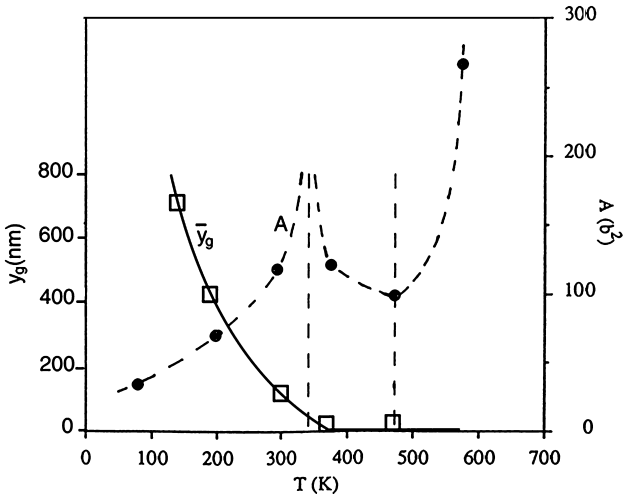

Figure 2 Temperature variation of the jump length $\bar{y}_g$ (*in situ* measurement) and activation area A (macroscopic data from [6]) in the medium-purity titanium.

parallel to each other, nor to the trace of any crystallographic plane containing the Burgers vector. Some short trace segments are however parallel to the trace of basal and pyramidal planes of the first order. It thus appears that extensive cross-slip has occurred.

Fig. 4 shows an **a**-dislocation gliding in a first-type pyramidal plane. Between Figs 4a and c, it makes a quick jump similar to those observed in the prismatic plane (Fig. 1). Here again, the initial and final positions of the jump can be seen on the same video frame (Fig. 4b). The occurrence of cross-slip is proved by the presence of many loops and debris.

3.3. Discussion

Rectilinear screw **a**-dislocations glide jerkily in prism planes as in beryllium and magnesium strained at low temperatures [1]. This behaviour has been attributed to alternate changes between two different core structures. When locked, dislocations have a stable and sessile core structure spread principally in the prismatic plane and secondarily in the basal one, according to the atomistic calculations of Legrand [9], and Girshick *et al.* [10]. The occurrence of jumps in the prismatic planes over distances longer than the distance between adjacent Peierls valleys is an indication that dislocations can also take a glissile and metastable core structure. Since the same type of motion has been observed in the pyramidal plane, another metastable core configuration may exist in this plane when the stress orientation is favourable. Dislocation glide

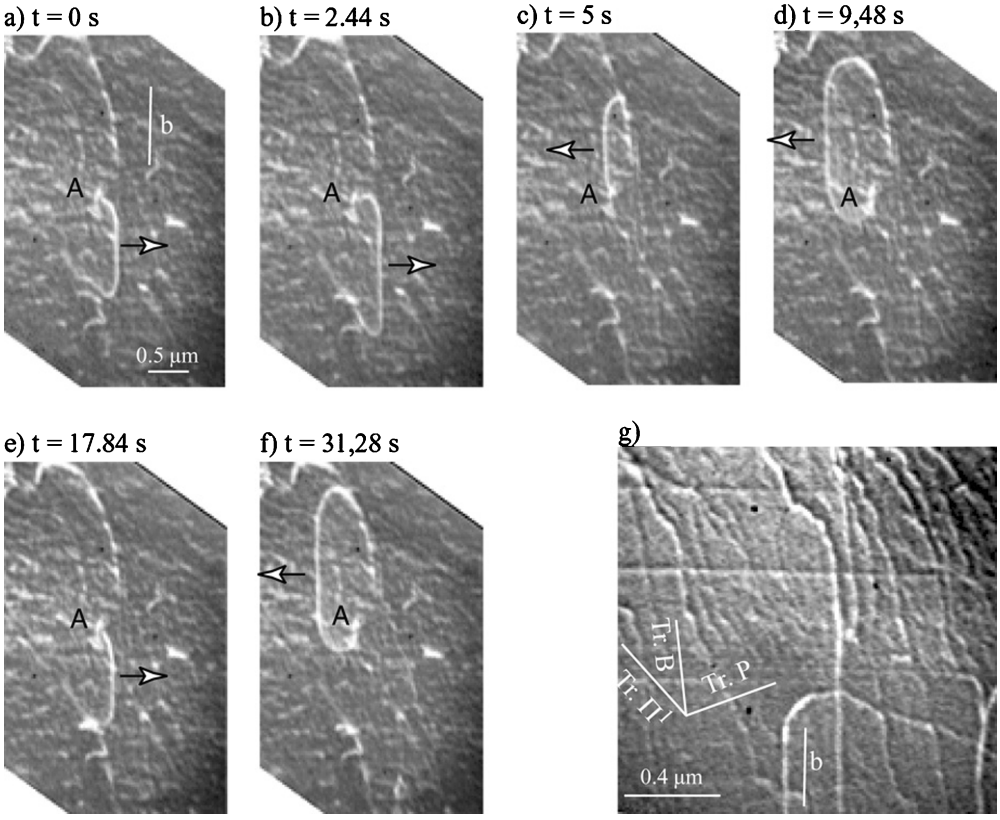

Figure 3 Source operating in the high-purity titanium strained at room temperature. *A* is the anchoring point and arrows indicate the direction of motion. Picture (*g*) shows the slip traces left by dislocations in this area. "Tr P" "Tr B" and "Tr Π^1" are the traces of the prismatic, basal and first type pyramidal planes, and b is the direction of the Burgers vector (in projection).

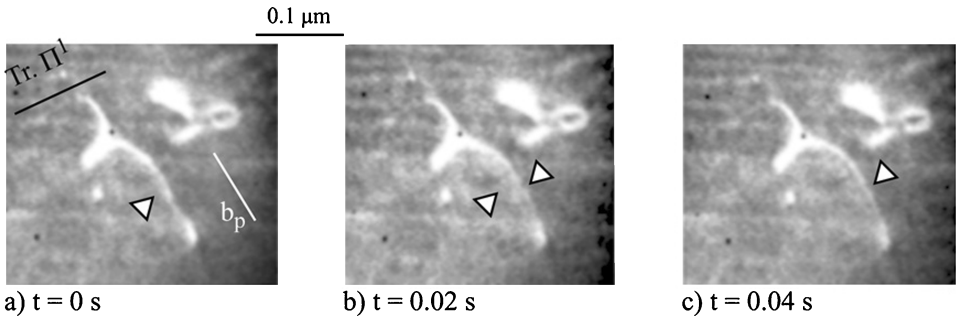

Figure 4 Glide of a **a**-dislocation in a first-type pyramidal plane. Arrows point to successive positions of screw segments, moving jerkily in (**b**).

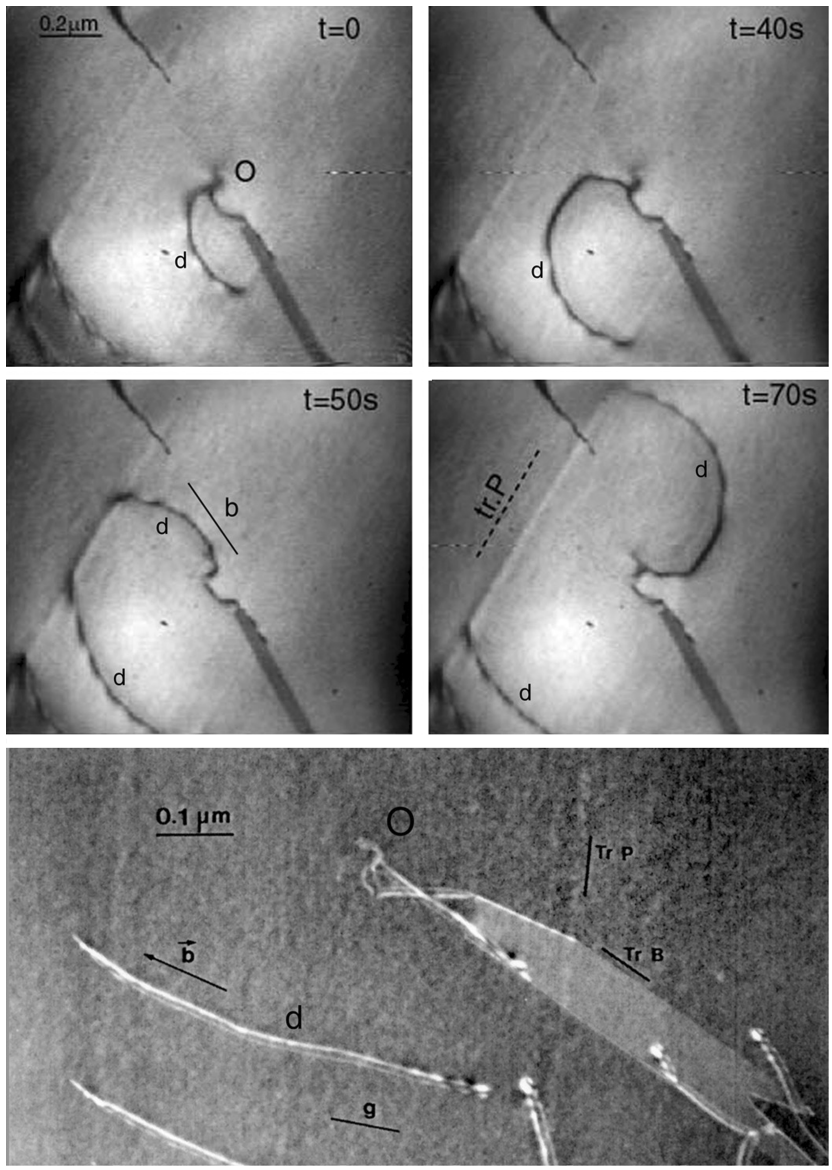

Figure 5 Dislocation source in a prismatic plane of Ti_3Al (*in situ* straining experiment at 300 K). *O* is the anchoring point, "tr P" is the trace of the prismatic plane, **b** is the direction of the Burgers vector (in projection), "tr B" is the trace of a stacking fault in the basal plane, and **g** is the diffraction vector $0\bar{2}21$. The dissociation width of the emitted dislocations is shown in the weak-beam picture.

in titanium can accordingly be described by the so-called "Locking-Unlocking mechanism" originally proposed to account for the prismatic glide of beryllium [12]. According to this description, dislocations undergo a series of thermally activated transitions between stable-sessile and metastable-glissile core configurations. The existence of several core configurations of different energies has been confirmed by Legrand [9], Girshick *et al*. [10] and Vitek and Igarashi [11]. It is clear that some of them can be more mobile in various planes than the most stable one. The existence of metastable-glissile configurations leading to a locking–unlocking mechanism instead of a pure Peierls one is considered as a general property of metals and alloys [13, 14].

As shown in Fig. 2, the jump length decreases as the temperature increases which is consistent with the locking probability, namely an increase of the frequency of the glissile to sessile transition. The peak in the temperature variation of the activation area arises when the jump length has decreased to a very small value, presumably equal to the interatomic distance, namely when the locking-unlocking mechanism reduces to the classical Peierls (or "kink-pair") mechanism. Details on this transition can be found in Farenc *et al*. [8], Caillard and Couret [13], Caillard and Martin [14].

4. Prism and basal glide in Ti_3Al

Gliding superdislocations have been observed in prismatic and basal planes of Ti_3Al polycrystals strained *in situ* between 300 K and 873 K [15, 16]. Some of their properties are described and discussed below.

4.1. Observations in prismatic planes

Plastic deformation is mostly due to the glide of superdislocations with $\frac{1}{3}\langle 11\bar{2}0\rangle$ Burgers vectors in $\{1\bar{1}00\}$ prismatic planes. Fig. 5 shows a source formed by a dislocation noted *d*. It rotates steadily around the anchoring point *O*, and emits curved dislocations in the prismatic plane which trace is labelled "Tr P". When observed under weak-beam conditions (last picture of Fig. 5), dislocations appear dissociated into two superpartials $\frac{1}{6}\langle 11\bar{2}0\rangle$. This dissociation mode is hereafter called "mode II".

In some cases, the behaviour of dislocations in prismatic planes is however definitely different. Fig. 6 shows a group of superdislocations gliding in a prismatic plane with trace "Tr P". Some of them exhibit the same rounded shape and narrow dissociation as above. Others however exhibit straight screw superpartial segments separated by a larger and variable dissociation widths. The rectilin-

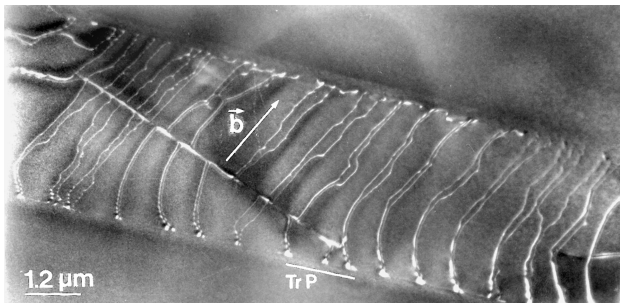

Figure 6 Slip band in a prismatic plane of Ti_3Al (*in situ* straining experiment at 300 K). "Tr P" is the trace of the prismatic plane, **b** denotes the screw orientation. Note the two dissociation modes, wide and bounded by straight screw superpartials (type I), and narrow and bounded by curved superpartials (type II).

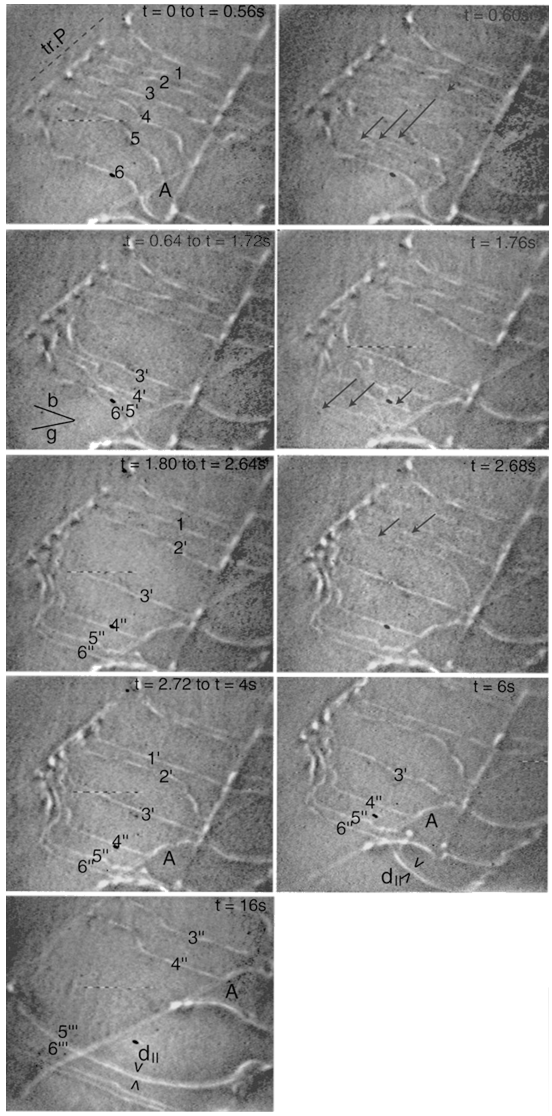

Figure 7 Sequence of glide in a type I prismatic plane of Ti_3Al (*in situ* straining experiment in weak-beam at 300 K). Superpartials are denoted by numbers from 1 to 6, and their successive positions are noted by superscripts prime, double prime etc. The slip trace is "tr P", and *A* is a fixed point. Dislocations remain immobile (left pictures) and suddenly jump to another locking position (right pictures, arrows). Note that one superdislocation changes from mode I ($5''$–$6''$) to mode II ($5'''$-$6'''$, narrow dissociation width d_{II}) in the two last pictures.

ear aspect of screw superpartials and the large scatter of the dissociation widths can be directly related to a high Peierls-type frictional force. This second dissociation mode is called "mode I". The continuity between both dislocation modes shows that the superpartials involved are the same (which has been verified by extinction experiments).

The kinetics of glide of type I dissociated dislocations is illustrated in Fig. 7. Superpartials 1 to 6 glide in the prismatic plane with trace "Tr P". They exhibit straight screw segments and are paired according to 1–2, 3–4, and 5–6. Screw segments remain immobile during one or several seconds, and suddenly jump very quickly to another sessile position, and so on. The jumps take place in a very short time, at least one order of magnitude shorter than 1/50 s (one frame of the video), because (i) only the corresponding starting and final positions are visible on the frame including the jump (see the two arrows in Fig. 7, at $t = 2.68$ s), (ii) the sum of the two corresponding contrast intensities is equal to that of the same dislocation before or after the jump, which shows that the total time is shared between the two locking positions, and (iii) one intermediate contrast can sometimes be observed on the same frame (see the three arrows at $t = 0.60$ s and $t = 1.76$ s), which shows that two fast jumps and one longer locking event have occurred within 1/50 s. Superdislocations can change their dissociation mode from type I (wide dissociation, straight screw segments) to type II (narrow dissociation, curved screw segments), as shown below. At $t = 6$ s, the superdislocation $5''$–$6''$ is partly dissociated in the mode I on the left side of the picture, and partly dissociated in the mode II on the right side (dissociation noted "d_{II}"). The "d_{II}" part moves between the two last pictures, as a result the whole superdislocation becomes curved and dissociated in the mode II.

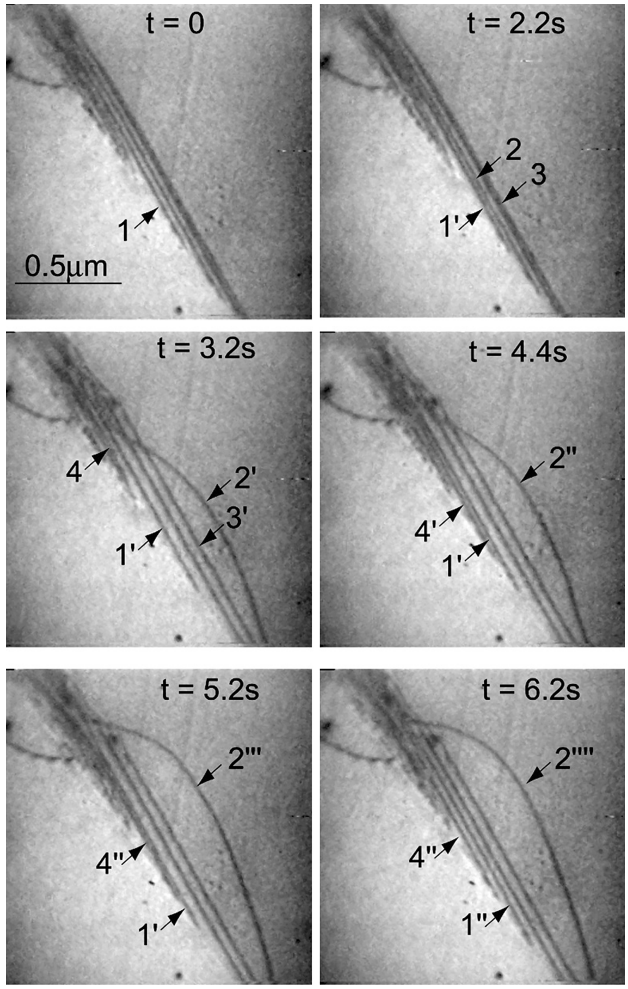

Figure 8 Sequence of glide in the basal plane of Ti_3Al (trace "tr B"), and cross-slip onto a type-II prismatic plane (*in situ* straining experiment at 473 K). Screw superdislocations move jerkily between locking positions (some of them are denoted by numbers from 1 to 4, and their successive positions are noted by superscripts prime, double prime etc). Note the change in the properties of superdislocation 2 when it cross slips onto the prismatic plane.

4.2. Observations in the basal plane

Basal glide is very planar. It involves the collective movement of dislocations with several Burgers vectors forming a network, as shown by Legros *et al.* [15, 16]. The situation is however simpler at the slip band heads, where straight screw superdislocations move jerkily like type I dislocations in the prismatic plane. Superdislocations 1, 3, 4 in Fig. 8 are seen in their different successive sessile positions. Meanwhile, superdislocation 2 escapes on the cross-slip prismatic plane. Because of its curved shape and steady motion, it obviously belongs to the type II dissociation mode. Such cross-slip events are frequent at the head of slip bands in the basal plane. They tend to form sources like in Fig. 5.

4.3. Discussion

The two dissociation modes in prismatic planes probably correspond to two different cutting planes, as expected from Blackburn [17], Umakoshi and Yamaguchi [18], and Cserti *et al.* [19]. The $D0_{19}$ structure is indeed made of alternate layers of Ti and TiAl prismatic dense planes between which two different planes of motion can be chosen. The nature of the first neighbour atoms remains unchanged after shear along the superpartial Burgers vector $\frac{1}{6}\langle 11\bar{2}0\rangle$ between two adjacent Ti planes, as a result the corresponding APB energy is low. In contrast, pairs of incorrect first nearest neighbours are made between adjacent TiAl planes, as a result the corresponding APB energy is higher. A comparison of the APB energies in prismatic, basal, and pyramidal planes, and the corresponding densities of incorrect first nearest neighbour atoms has been made recently by Legros and Caillard [20]. It shows that the density of incorrect first nearest neighbours is an important contribution to the APB energy, but that more distant interactions must also be taken into account.

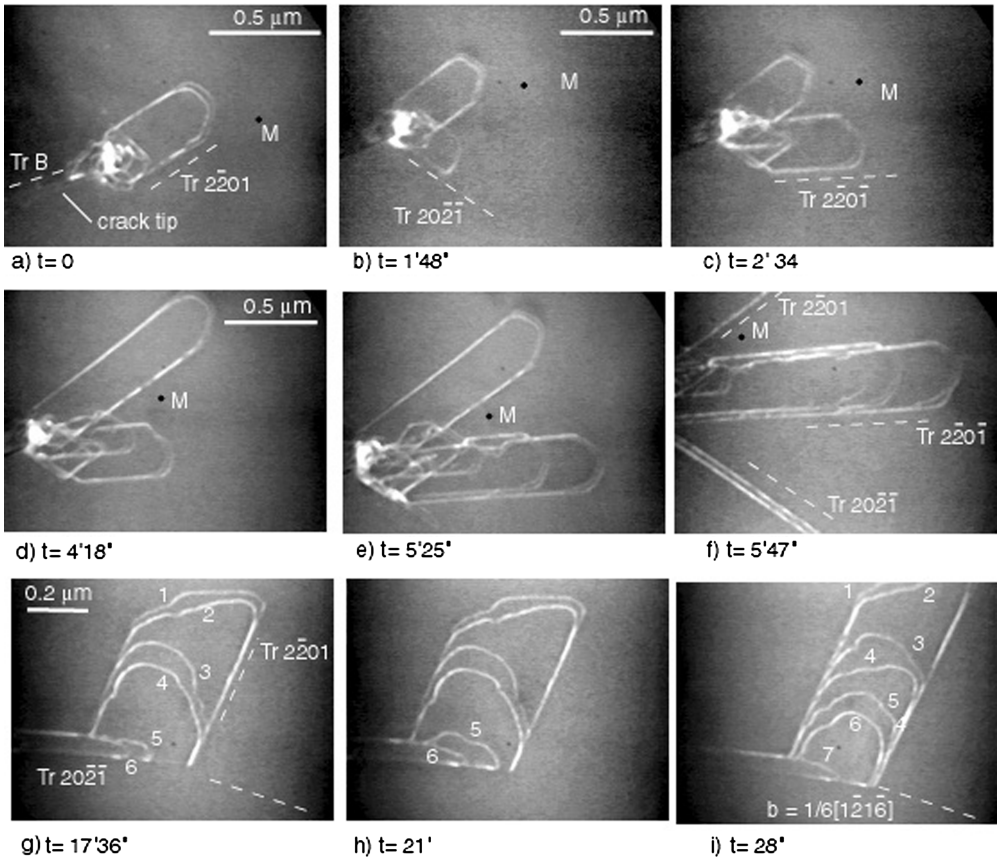

Figure 9 Emission of 2**c** + **a** dissociated superdislocations from the head of a crack-tip located in the basal plane. *In situ* straining experiment at 473 K, along the **c**-direction. (a)–(f): Video frames: one 2**c** + **a** superdislocation is emitted in each of the three slip systems successively activated. M is a fixed point. (g)–(i): video frames showing the cross-slip of a pile-up of **c** + **a**/2 superpartial dislocations between two π_1 planes. The direction of the Burgers vector (image (i)) is parallel to the intersection of the two glide planes (dotted line). Superpartials 6 and 7 are seen to straighten along this direction before cross-slipping.

The jerky motion of screw dislocations in basal and prismatic (type I) planes is ascribed to a locking-unlocking mechanism like in pure Ti (Section 3). It involves a non-planar superpartial core structure, obtained with the atomistic calculations of Cserti *et al*. [19]. The core structure of type II screw segments should conversely be planar, but it has unfortunately not been computed.

It is interesting to note that the behaviour of screw dislocations in the type I prismatic planes bounded by Ti atoms only is the same as in pure Ti (see Section 2), and that the corresponding core structures are similar. This shows that the dislocation core structure is strongly influenced by the nature of its nearest constituent atoms (Ti, or Ti + Al). It is also interesting to note that dislocations gliding in the basal plane tend to cross slip on the prismatic plane of highest APB energy (narrowest dissociation width) where they can move more easily (no frictional force). This shows that dislocation mobility is sometimes more important than dislocation energy alone, in the competition between different glide mechanisms.

5. Pyramidal glide in Ti_3Al

5.1. Experimental results

Pyramidal glide of 2**c** + **a** dislocations has been observed between 120 and 473 K (Legros [21], Legros, Minonishi, and Caillard [22, 23]). Since the CRSS of pyramidal slip is much higher than those of prismatic and basal slip, it is usually necessary to strain the single crystal along the **c**-axis to activate pyramidal slip. The pyramidal planes sheared in compression are always of the second type, ($\{11\bar{2}2\}$, hereafter called π_2), whereas only the first type pyramidal planes, ($\{2\bar{2}01\}$ hereafter called π_1) have been observed in tension. The Ti_3Al single crystals that have been *in situ* strained along the **c**-axis in this study were provided by Y. Minonishi from Tohoku University in Sendai (Japan).

Fig. 9 is an *in situ* video sequence taken at 473 K, showing the emission of 2**c** + **a** superdislocations from a crack-tip belonging to the basal plane. The strain axis is perpendicular to the basal plane. As a result, the Schmid factor is zero for basal and prismatic glide of **a** dislocations. From Fig. 9a–f, three slip systems are successively activated on $(2\bar{2}01)$,$(20\bar{2}\bar{1})$, and $(2\bar{2}0\bar{1})$ π_1-type

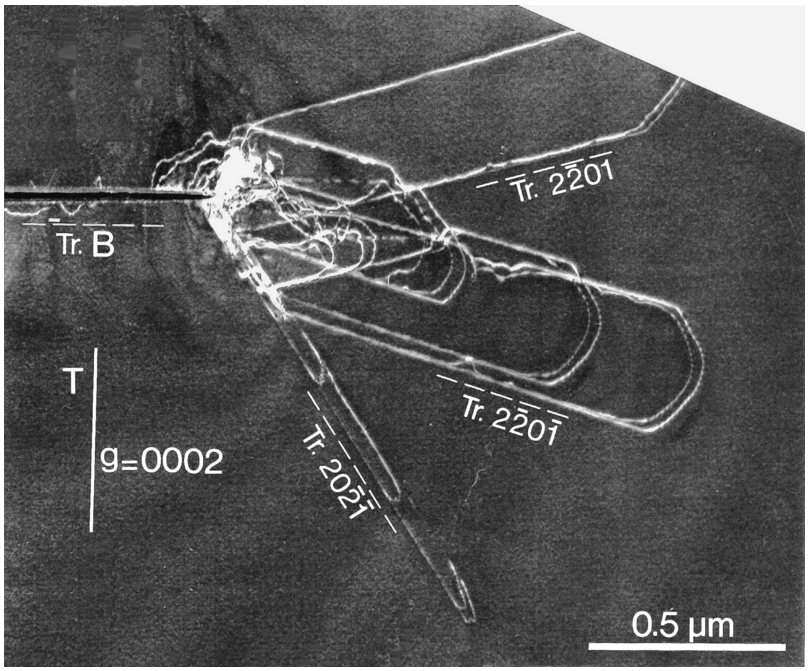

Figure 10 Still micrograph corresponding to Fig. 9e. Note that most of the pyramidal planes are sheared with only one $2\mathbf{c} + \mathbf{a}$ superdislocation except for $(2\bar{2}0\bar{1})$ where two widely separated superpartials follow the leading superdislocation. This pile-up is at the origin of the cross-slip seen on Fig. 9g–i. Each dislocation line corresponds to a $\mathbf{c} + \mathbf{a}/2$ superpartial.

pyramidal planes. Pairs of $\mathbf{c} + \mathbf{a}/2$ superpartial dislocations appear suddenly and travel several hundreds of nanometers before they stop. Fig. 10 is a still micrograph that gives an overview of the three pyramidal systems ahead of the crack tip at $t = 5'25''$. When further straining is applied, dislocations gliding on $(20\bar{2}\bar{1})$ cross-slip onto $(2\bar{2}01)$ (Fig. 9g–i). One can note that all the superdislocations of the same plane cross slip at the same location.

Cusps on dislocation lines are also visible on Fig. 9g–i taken at a higher magnification. Pinning actually occurs on rows of loops that have been nucleated by the leading superpartials, and that are labelled *X*, *Y* and *Z* accordingly to Legros *et al*. [22, 23]. When the diffracting vector $\mathbf{g} = 0002$ is used (Fig. 11a and b), *Z* loops are visible but *X* and *Y* ones are out of contrast. On the contrary, when the diffracting vector pertains to the basal plane (Fig. 11c and d), *Z* loops are out of contrast while *X* and *Y* loops are visible. The π_1 pyramidal planes contain three potential Burgers vectors that are $\mathbf{c} + \mathbf{a}_1/2$, $\mathbf{c} + \mathbf{a}_2/2$, and $\mathbf{a}_3$, where $\mathbf{a}_1$, $\mathbf{a}_2$ and $\mathbf{a}_3$ are the three $1/3\langle 11\bar{2}0\rangle$ directions contained in the basal plane. In the experiments reported here, only one Burgers vector was activated at a time. If we denote the Burgers vector of the gliding superpartials by $\mathbf{c} + \mathbf{a}_1/2$, the direction on which the loops are aligned is always $\mathbf{c} + \mathbf{a}_2/2$. The Burgers vector of the *X* and *Y* loops are proportional to $\mathbf{a}_2$ and $\mathbf{a}_1$, respectively, while *Z* loops are of **c** type. Since none of these Burgers vectors belongs to the glide plane, the three types of loops are prismatic.

The nucleation of *X*, *Y* and *Z* loops is a complex mechanism that has been described elsewhere [23]. Post mortem and *in situ* experiment analysis indicated that *X* loops are the first to form in the trail of the first superpartials of the pile-up and are therefore responsible for the alignment of the loops along $\mathbf{c} + \mathbf{a}_2/2$. The nucleation of these loops and their interaction with the following dislocations of the pile-up is accentuated when the dislocation line is perpendicular to $\mathbf{c} + \mathbf{a}_2/2$. This situation is clearly illustrated by Fig. 12 on which a pile-up of seven $\mathbf{c} + \mathbf{a}_1/2$ superpartials glide in a π_1 pyramidal plane. The diffraction vector does not reveal *X* and *Y* loops but one can notice that segments *B*, perpendicular to the $\mathbf{c} + \mathbf{a}_2/2$ direction are heavily cusped. This phenomenon increases as we consider dislocations further away from the head of the pile-up. On the contrary, dislocation segments *A*, whose line is parallel to the $\mathbf{c} + \mathbf{a}_2/2$ direction are constantly smooth. Finally, one can note that the wide dissociation of the leading superdislocation (typically 50 nm along the smooth $\mathbf{c} + \mathbf{a}_2/2$ direction) becomes even wider when looking to the back of the pile-up. The last superpartial on this picture can actually be considered as unpaired since the following and matching superpartial is more than 1 μm away (not seen in the picture).

5.2. Discussion

5.2.1. Tension-compression asymmetry

The tension-compression asymmetry along the **c**-axis has been first revealed in Ti_3Al by mean of *in situ* straining

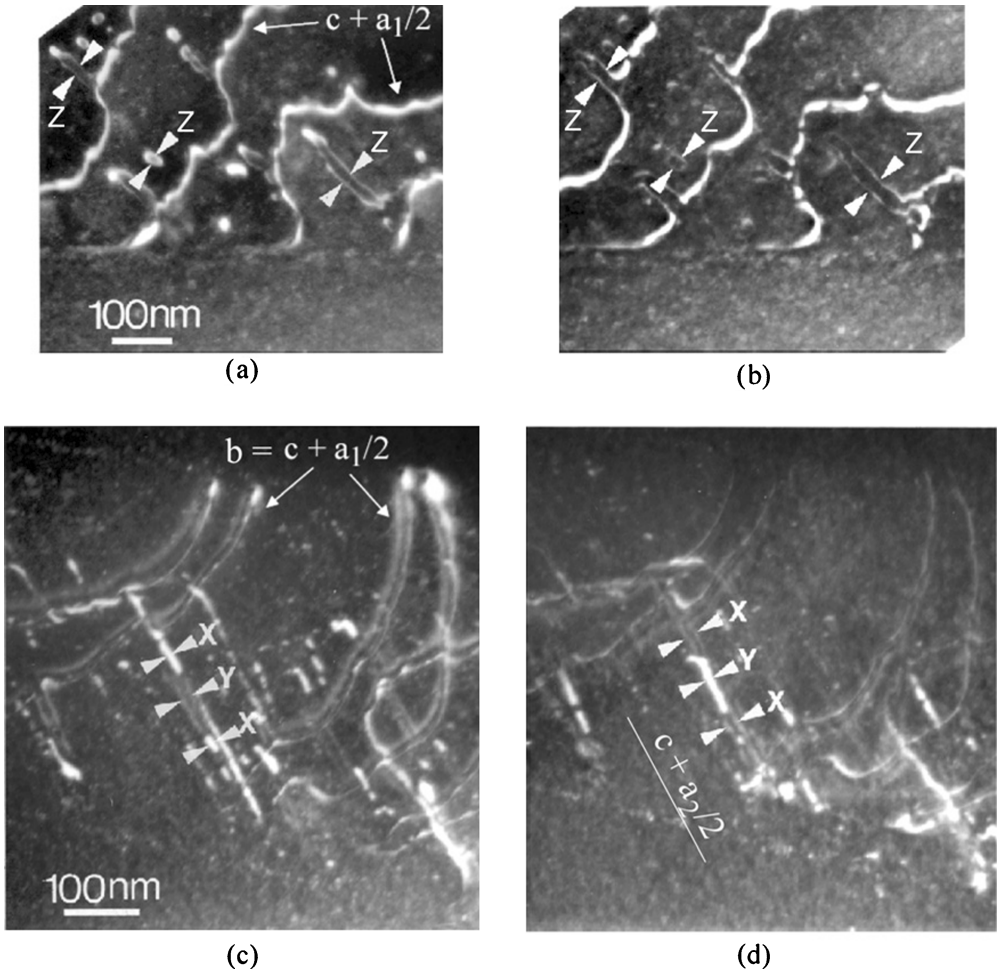

Figure 11 Interaction of moving $\mathbf{c} + \mathbf{a}_1/2$ dislocations with rows of prismatic loops in a π_1 pile-up (*in situ* straining experiment at 300 K). (a), (b): *Z* loops (Burgers vector along the **c**-direction) are imaged using $g = \pm 0002$. (c), (d): *X* and *Y* loops are imaged using $g = \pm 22\bar{4}0$. These loops are prismatic because they have Burgers vectors proportional to $\mathbf{a}_1$ and $\mathbf{a}_2$, respectively, while only $\mathbf{a}_3$ is contained in the π_1 glide plane. Note the direction of alignment $\mathbf{c} + \mathbf{a}_2$.

experiments [22, 23]. The possible thin foil effects in such observations have been discussed by Minonishi *et al*. [24]. However, this was definitely ruled out by the results of Kishida *et al*. [25] who confirmed that π_1 glide was activated in bulk specimens deformed in tension whereas π_2 glide was operating in compression. A change in slip plane depending on the sense of the applied stress may occur when the crystallographic conditions for an equivalent shear in two opposite directions, such as defined by Kelly and Groves [26], are not fulfilled. This is the case in hcp and $D0_{19}$ structures where neither the directions normal to π_1 and π_2 pyramidal planes nor the Burgers vector direction ($\mathbf{c} + \mathbf{a}/2$) are parallel to an axis of evenfold symmetry. Computer simulations using Lennard-Jones a two body potential have also shown that the $\mathbf{c} + \mathbf{a}$ (equivalent to $\mathbf{c} + \mathbf{a}/2$ in the $D0_{19}$ structure) screw dislocations in a model hcp metal exhibit several core structures that are all asymmetric with respect to a 180° rotation around their line direction or slip plane normal [27]. These simulations also indicate that these dislocations glide in π_1 planes when the crystal is strained along the *c*-axis in tension and along π_2 planes when the load is reversed to compression. Finally, a change of the slip plane upon load inversion has been identified in Ti (Minonishi *et al*. [28]). This slip asymmetry observed in Ti_3Al may therefore be a characteristic of both hcp disordered and ordered metals and alloys. It is interesting to note that for a given alloy composition, the CRSS values for π_1 and π_2 slip are very close to each other [25]. This fact, combined with the resemblance of observed $\mathbf{c} + \mathbf{a}/2$ dislocations on both types of planes (Court *et al*. [29], Legros *et al*. [22, 23]), suggests that a unique controlling mechanism governs the pyramidal glide of $\mathbf{c} + \mathbf{a}/2$ dislocations in Ti_3Al and possibly that of $\mathbf{c} + \mathbf{a}$ dislocations in Ti.

5.2.2. Behaviour of $\mathbf{c} + \mathbf{a}/2$ dislocations in π_1 planes

Although Kishida *et al*. [25] could not clearly identify the Burgers vectors involved in π_1 slip, they assumed it to be

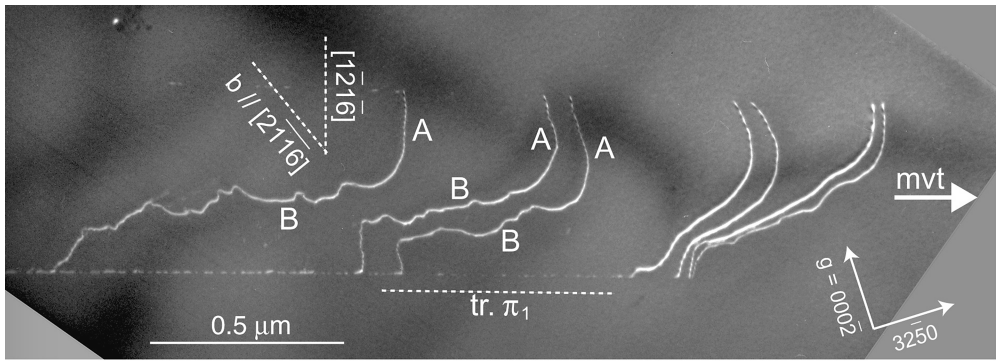

Figure 12 Head of a slip band in the $(2\bar{2}01)\,\pi_1$ pyramidal plane. $1/6[2\bar{1}\bar{1}\bar{6}] = \mathbf{c} + \mathbf{a}_1/2$ is the Burgers vector of the mobile dislocations, whereas $1/6[1\bar{2}1\bar{6}] = bfc + \mathbf{a}_2/2$ is the direction of loop alignment (out of contrast with $\mathbf{g} = 0002$). The dissociation of superdislocations widens as one moves away from the head of the pile-up. Note that segments A, parallel to $\mathbf{c} + \mathbf{a}_2/2$, are smooth whereas segments B, perpendicular to $\mathbf{c} + \mathbf{a}_2/2$, are heavily cusped. *In situ* straining experiment at 300 K.

of $2\mathbf{c} + \mathbf{a}$ type. Surface monitoring of macroscopically deformed samples revealed that shearing of π_1 planes was very localized, which is in good agreement with our *in situ* observations showing large pile-ups of coplanar $\mathbf{c} + \mathbf{a}/2$ dislocations [21, 22]. Dislocations in these pile-ups cross slip onto another plane at the same exact location and thus maintain the coplanar aspect of the deformation (Fig. 9). This behaviour may be the result of a local disordering of the glide plane induced by the glide of $\mathbf{c} + \mathbf{a}/2$ superpartials [23]. This disordering is evidenced by the wider dissociation of successive superdislocations in pile-ups, as seen on Fig. 12. This dissociation is inversely proportional to the anti-phase boundary (APB) energy which depends on the local degree of order of the crystal.

It has been suggested that the mobility of $2\mathbf{c} + \mathbf{a}$ dislocations was controlled by a Peierls-type interaction of the dislocation line with the crystal lattice. Such a strong interaction, resulting from covalent bonds along certain directions of the Ti_3Al $D0_{19}$ structure [29], would lead to the observation of straight $2\mathbf{c} + \mathbf{a}$ edge dislocations. This has never been observed, however. On the contrary, dislocations are pinned at many points corresponding to the nucleation of dislocation loops. As mentioned before, π_1 pyramidal planes contain three potential Burgers vectors noted $\mathbf{c} + \mathbf{a}_1/2$, $\mathbf{c} + \mathbf{a}_2/2$ and $\mathbf{a}_3$. Dislocations with a Burgers vector $\mathbf{c} + \mathbf{a}_1/2$ nucleate X and Z prismatic loops aligned along the $\mathbf{c} + \mathbf{a}_2/2$ direction, as a result the linear density of pinning points is the highest (and the dislocation mobility is the lowest) along the direction perpendicular to $\mathbf{c} + \mathbf{a}_2/2$. In the pile-up, the motion of following $\mathbf{c} + \mathbf{a}_1/2$ dislocations is hindered by their interaction with these loops, which intensifies the pinning and explains the occurrence of long cusped segments perpendicular to the $\mathbf{c} + \mathbf{a}_2/2$ direction (see Fig. 12).

5.2.3. Dislocation emission from a crack tip

The weak-beam conditions allow one to resolve many details of the dislocation structure at the crack tip, in spite of strong lattice distortions (Figs 9 and 10). There is a high density of tangled dislocations from which individual $\mathbf{c} + 2\mathbf{a}$ superdislocations emerge rapidly in several pyramidal planes. The c-components of their Burgers vectors obviously contribute to relaxing the stress concentration at the crack tip. Several superdislocations have been emitted in the same plane, which shows that they originate from the same source, presumably a Frank-Read source in the tangled area. Under such conditions, the rate of emission appears to be limited by the high local strain hardening due to the tangling, rather than by the nucleation of new dislocations at the crack surfaces.

6. General discussion and concluding remarks

The present results emphasise the advantages of *in situ* experiments to study complex dislocation mechanisms like those involved in the plasticity of hcp metals and alloys. Indeed, metastable glissile dislocation core structures, which allow long jumps between sessile positions in prismatic planes, cannot be observed by conventional electron microscopy. In the same way, a series of complex dislocation reactions in pyramidal planes, leading to the formation of defects with three Burgers vectors all different from that of the mother dislocations, could not be reconstituted on the basis of still pictures only.

The dislocation behaviour in Ti and Ti_3Al exhibits several analogies and differences. Superdislocations in the prismatic planes of Ti_3Al have the same kinetics as dislocations in the prismatic planes of Ti, provided they glide in the layers bounded by Ti atoms only. Those gliding in layers bounded by Ti and Al atoms behave differently. This shows that (i) superpartials in Ti/Ti prismatic layers of Ti_3Al have the same core structure as dislocations in prismatic planes of Ti, and (ii) the dislocation core structure in Ti_3Al depends strongly on the nature of its nearest atoms. Pyramidal slip in Ti_3Al and in Ti is presumably similar because the same tension-compression asymmetry occurs.

In both materials, the mechanical properties depend directly on the dislocation core structures. No covalent bonding effect has been found in Ti_3Al. The CRSS of prismatic slip in Ti and the corresponding strain rate sensitivity of the stress (activation area) are determined by the sessile and metastable-glissile core structures of **a** dislocations. Although the same mechanism has been observed in the type I prismatic planes of Ti_3Al, the corresponding CRSS is more likely determined by the glissile core structure in type II planes. The CRSS of pyramidal glide in Ti_3Al is determined by a new mechanism: the self nucleation of small-size obstacles. Indeed, glide can no more be considered as a pure shear mechanism leaving the structure unchanged. On the contrary, glide is accompanied by irreversible atomic displacements which generate small-size obstacles to dislocation motion, and induce some disorder in the slip plane (decrease of APB energy). Such self-nucleated obstacles have never been reported before, to the author's knowledge. Less pronounced glide-induced disordering has been previously observed in Ni_3Al by Horton *et al*. [30] but no self-nucleated obstacle was reported. The self-nucleation of small-size obstacles may operate in any material containing dislocations with large Burgers vectors, provided stacking fault energies are too high to permit a wide dissociation. Indeed, lattice distortions may be large enough in dislocation cores to induce similar irreversible atomic displacements.

References

1. A. COURET, D. CAILLARD, W. PÜSCHL and G. SCHOECK, *Phil. Mag. A* **63** (1991) 1045.
2. H. NUMAKURA and M. KOIWA, *Metal. Sci. Tech.* **16** (1998) 4.
3. A. COURET, J. CRESTOU, S. FARENC, G. MOLÉNAT, N. CLÉMENT, A. COUJOU and D. CAILLARD, *Microsc. Microanal. Microstruct.* **4** (1993) 153.
4. F. PETTINARI, A. COURET, D. CAILLARD, G. MOLÉNAT, N. CLÉMENT and A. COUJOU, *J. Microsc.* **203** (2001) 47.
5. M. P. BIGET and G. SAADA, *Phil. Mag. A* **59** (1989) 747.
6. S. NAKA, A. LASALMONIE, P. COSTA and L. P. KUBIN, *ibid.* **57** (1991) 717.
7. S. FARENC, D. CAILLARD and A. COURET, *Acta Metall. Mater.* **41** (1993) 2701.
8. S. FARENC, D. CAILLARD and A. COURET, *ibid.* **43** (1995) 3669.
9. B. LEGRAND, *Phil. Mag. A* **52** (1985) 83.
10. A. GIRSHICK, D. G. PETTIFOR and V. VITEK, *ibid.* **77** (1998) 999.
11. V. VITEK and M. IGARASHI, *ibid.* **63** (1991) 1059.
12. A. COURET and D. CAILLARD, *ibid.* **59** (1989) 783.
13. D. CAILLARD and A. COURET, *Mat. Sci. Eng.* **A322** (2002) 108.
14. D. CAILLARD and J. L. MARTIN, "Thermally Activated Dislocation Mechanisms in Crystal Plasticity," edited by R. W. Cahn (Pergamon Materials Series, 2003).
15. M. LEGROS, A. COURET and D. CAILLARD, *Phil. Mag. A* **73** (1996) 61.
16. M. LEGROS, A. COURET and D. CAILLARD, *ibid.* **73** (1996) 81.
17. M. J. BLACKBURN, *Trans. Metall. Soc. AIME* **239** (1967) 660.
18. Y. UMAKOSHI and M. YAMAGUCHI, *Phys. Stat. Sol. (a)* **68** (1981) 457.
19. J. CSERTI, M. KHANTA, V. VITEK and D. P. POPE, *Mater. Sci. Eng. A* **152** (1992) 95.
20. M. LEGROS and D. CAILLARD, *J. Microsc.* **203** (2001) 90.
21. M. LEGROS, Thèse no 1739, Université Paul Sabatier, 1994.
22. M. LEGROS, Y. MINONISHI and D. CAILLARD, *Phil. Mag. A* **76** (1997) 995.
23. *Idem.*, *ibid.* **76** (1997) 1013.
24. Y. MINONISHI, M. LEGROS and D. CAILLARD, *MRS Symp. Proc.* **460** (1997) 237.
25. K. KISHIDA, J. YOSHIKAWA, H. INUI and M. YAMAGUCHI, *Acta Metall. Mater.* **47** (1999) 3405.
26. A. KELLY and G. W. GROVES, "Crystallography and Crystal Defects" (Longman, London, 1970) p. 174.
27. Y. MINONISHI, S. ISHIOKA, M. KOIWA and S. MOROZUMI, *Phil. Mag. A* **46** (1982) 761.
28. Y. MINONISHI, S. MOROZUMI and H. YOSHINAGA, *Scripta Met.* **16** (1982) 427.
29. S. A. COURT, J. P. A. LOFVANDER, M. H. LORETTO and H. L. FRASER, *Phil. Mag. A* **61** (1990) 109.
30. J. A. HORTON, I. BAKER and M. H. YOO, *ibid.* **63** (1991) 319.